The Hv1 proton channel responds to mechanical stimuli

Medha M. Pathak,[1]* Truc Tran,[1]* Liang Hong,[1] Béla Joós,[2] Catherine E. Morris,[3] and Francesco Tombola[1]

[1]Department of Physiology and Biophysics, University of California, Irvine, CA 92697
[2]Department of Physics, University of Ottawa, Ottawa, Ontario K1N 6N5, Canada
[3]Ottawa Hospital Research Institute, Ottawa, Ontario K1H 8M5, Canada

The voltage-gated proton channel, Hv1, is expressed in tissues throughout the body and plays important roles in pH homeostasis and regulation of NADPH oxidase. Hv1 operates in membrane compartments that experience strong mechanical forces under physiological or pathological conditions. In microglia, for example, Hv1 activity is potentiated by cell swelling and causes an increase in brain damage after stroke. The channel complex consists of two proton-permeable voltage-sensing domains (VSDs) linked by a cytoplasmic coiled-coil domain. Here, we report that these VSDs directly respond to mechanical stimuli. We find that membrane stretch facilitates Hv1 channel opening by increasing the rate of activation and shifting the steady-state activation curve to less depolarized potentials. In the presence of a transmembrane pH gradient, membrane stretch alone opens the channel without the need for strong depolarizations. The effect of membrane stretch persists for several minutes after the mechanical stimulus is turned off, suggesting that the channel switches to a "facilitated" mode in which opening occurs more readily and then slowly reverts to the normal mode observed in the absence of membrane stretch. Conductance simulations with a six-state model recapitulate all the features of the channel's response to mechanical stimulation. Hv1 mechanosensitivity thus provides a mechanistic link between channel activation in microglia and brain damage after stroke.

The Journal of General Physiology

INTRODUCTION

The Hv1 protein (a.k.a. HVCN1 or VSOP) consists of a proton-conducting voltage-sensing domain (VSD) connected to a coiled-coil domain (CCD) that mediates dimerization (Ramsey et al., 2006; Sasaki et al., 2006; Li et al., 2010; Fujiwara et al., 2012). As a result, the channel has two VSD subunits and two gated proton permeation pathways that open and close cooperatively (Koch et al., 2008; Lee et al., 2008; Tombola et al., 2008, 2010; Gonzalez et al., 2010; Musset et al., 2010b). The Hv1 VSD is similar to the corresponding domain of voltage-gated potassium, sodium, and calcium channels and voltage-sensitive phosphatases (Long et al., 2005; Payandeh et al., 2011; Zhang et al., 2012; Li et al., 2014; Takeshita et al., 2014). The domain is made of four membrane-spanning segments, S1–S4, with the fourth segment providing the major contribution to the gating charge (Gonzalez et al., 2013; Chamberlin et al., 2014).

Because of its roles in human health and disease (DeCoursey, 2013; Pupo and Gonzalez León, 2014; Seredenina et al., 2015), Hv1 is an emerging drug target for cancer and stroke. The channel is found in cellular compartments that experience strong mechanical forces, such as the apical membrane of airway epithelial cells (Iovannisci et al., 2010), where motile cilia beat in coordinated waves, and the flagellar tail of sperm cells (Lishko et al., 2010). In highly metastatic breast cancer cells, Hv1 is involved in the intensely mechanical process of cell migration (Wang et al., 2011, 2012; McGrail et al., 2015). In phagocytic cells, including neutrophils, macrophages, and microglia, Hv1 is present on both the plasma membrane and phagosomes, where it modulates the production of reactive oxygen species (ROS) by NOX enzymes to kill engulfed pathogens (DeCoursey, 2013). The plasma membrane of these cells experiences mechanical forces during spreading (Henry et al., 2015), migration (Houk et al., 2012), and phagocytosis (Masters et al., 2013). The transmembrane protein complex NOX generates reactive superoxide anions by transferring electrons from NADPH to oxygen molecules. The process causes cytoplasmic accumulation of protons and membrane depolarization, both of which inhibit NOX activity (Henderson et al., 1987; Morgan et al., 2005). Hv1 promotes sustained NOX activity by extruding excess cytoplasmic protons and by counteracting membrane depolarization (DeCoursey, 2013).

We wondered whether Hv1 activity could be modulated by mechanical forces. Because voltage-gated potassium and sodium channels were previously reported to be sensitive to membrane stretch (Laitko et al., 2006;

*M.M. Pathak and T. Tran contributed equally to this paper.
Correspondence to Francesco Tombola: ftombola@uci.edu
Abbreviations used: CCD, coiled-coil domain; HSPC, high-speed pressure clamp; ROS, reactive oxygen species; VSD, voltage-sensing domain.

The Rockefeller University Press $30.00
J. Gen. Physiol. 2016 Vol. 148 No. 5 405–418
https://doi.org/10.1085/jgp.201611672

Beyder et al., 2010; Schmidt et al., 2012; Morris et al., 2015), we investigated the response of Hv1 to this particular type of mechanical stimulus. We found that membrane stretch strongly affects Hv1 gating and that the channel's activation rate is the most mechanosensitive parameter. Our findings are consistent with a scenario in which Hv1 switches to a "facilitated" mode upon mechanical stimulation. Once in this mode, the channel can be opened by smaller membrane depolarizations. We also found that membrane stretch affects a form of Hv1 lacking the CCD and previously shown to be monomeric (Koch et al., 2008; Tombola et al., 2008; Fujiwara et al., 2013). A comparison of how dimeric and monomeric forms of Hv1 respond to membrane stretch showed that, although the channel's VSD is intrinsically mechanosensitive, interactions between the two subunits in the dimeric complex modulate VSD mechanosensitivity. The behavior of monomeric Hv1 was reproduced by a four-state model in which the mechanical stimulus induced transitions increasing the rate of channel opening and the channel maximal conductance. Two additional states were necessary to simulate the long-lasting effects of membrane stretch on dimeric Hv1 activation.

Microglial cells exposed to brain damage experience intracellular acidification (Siesjö et al., 1996; Xiong et al., 2004) and cell swelling (Mongin, 2007; Song and Yu, 2014), which lead to Hv1 hyperactivation (Morihata et al., 2000). Our findings provide a direct mechanism linking cell swelling to Hv1 hyperactivation via membrane stretch. The mechanosensitivity of the Hv1 protein is particularly relevant in the context of ischemic stroke because excessive activity of the microglial channel is known to enhance neuronal death via NOX-mediated ROS production (Wu et al., 2012).

MATERIALS AND METHODS

Plasmid constructions

Human Hv1 constructs were generated as described previously, by subcloning cDNA of the Hv1 channel (provided by D. Clapham [Harvard University, Cambridge, MA; Ramsey et al., 2006] and from IMAGE clone 5577070 [Open Biosystems]) into the pGEMHE vector (Liman et al., 1992). In the $Hv1NC_{VSP}$ chimera, residues 1–96 and 228–273 of Hv1 were replaced by residues 1–113 and 240–576 of Ci-VSP, respectively (Murata et al., 2005), as described previously (Hong et al., 2013).

Channel expression in *Xenopus laevis* oocytes

Plasmids were linearized with either NheI or SphI (New England Biolabs, Inc.) before in vitro transcription with a T7 mMESSAGE mMACHINE transcription kit (Ambion). RNA quality was confirmed by running a denaturing RNA gel. mRNAs were injected in *Xenopus* oocytes (50 nl per cell, 0.3–1.5 µg/µl; Ecocytes Biosciences), and electrophysiological measurements were performed 1–3 d later. Cells were maintained at 18°C in ND96 medium (96 mM NaCl, 2 mM KCl, 1.8 mM $CaCl_2$, 1 mM $MgCl_2$, 5 mM HEPES, 5 mM pyruvate, and 100 µg/ml gentamycin at 18°C, pH 7.2).

Patch clamp recordings

After 1–4 d, the oocytes injected with mRNA were examined under patch clamp configuration. Patch measurements were performed in excised inside-out configuration, using an Axopatch 200B patch clamp amplifier set up on an IX71 microscope (Olympus). Pipettes had 2–4 MΩ access resistance in our solutions. The bath solution was composed of 100 mM Mes buffer, 30 mM TEA methanesulfonate, 5 mM TEA chloride, 5 mM EGTA, adjusted to pH 6.0 with TEA hydroxide. For recordings performed in the absence of pH gradient (pH_i and pH_o 6.0), the pipette solution had the same composition of the bath solution. Some of the measurements were performed in the presence of a pH gradient (pH_i 6.0 and pH_o 7.5). In these cases, the extracellular solution contained 100 mM HEPES, 40 mM TEA methanesulfonate, and 5 mM TEA chloride, adjusted to pH 7.5 with TEA hydroxide. Current traces were filtered at 1 kHz, digitized at 5 kHz, and analyzed with Clampfit 10.2 (Molecular Devices) and Origin 8.1 (OriginLab). All measurements were performed at 22 ± 2°C.

Mechanical stimulation of membrane patches

Mechanical stimulation of excised inside-out patches was performed with a high-speed pressure clamp (HSPC-1; ALA Scientific) controlled by pCLAMP 10.2. Suction pulses were administered to the membrane patch through the patch pipette connected to the HSPC-1.

Data analysis

Analysis of data was performed using Clampfit (version 10; Molecular Devices) and Origin (version 8; OriginLab). G-V plots were fitted with the Boltzmann equation $G/G_{max} = 1/[1 + \exp((V_{1/2} - V)/s)]$, where $V_{1/2}$ is the potential of half-maximal activation and s is the slope parameter. Time constants of activation (τ_a) and deactivation (τ_d) were obtained by fitting the currents to an exponential function of the form $I(t) = b + a * \exp(-t/\tau)$. In Figs. 3 and 4, $EP = 100 * (I_{EP} - I_{P0})/I_{P0}$, where I_{EP} is the current measured at the end of the pressure pulse and I_{P0} is the corresponding isochronal current measured in the absence of the pulse. Similarly, $ED = 100 * (I_{ED} - I_{D0})/I_{D0}$, where I_{ED} is the current measured at the end of the depolarization step in the presence of the pressure pulse and I_{D0} is the corresponding isochronal current measured in the absence of the pulse. Unless otherwise stated, data are represented as mean ± SEM. Effect of pressure stimuli on patches was

statistically examined by comparing control conditions and the presence of pressure using the paired *t* test. P-values <0.05 are considered statistically significant.

Modeling

The modeling results shown in Fig. 7 were obtained using the two-, four-, and six-state kinetic models illustrated in Fig. S1. The rate constants are given in Tables S1, S2, and S3. For dimeric Hv1, the relative values of the rate constants were determined from the experimentally obtained G-V curves (see Fig. 1 F) and then fitted to obtain the correct rate constants (Tables S1 and S2). For monomeric Hv1, a four-state model based on the dimer model reproduced the data very well once the rate constants were scaled to reflect the much faster kinetics of the monomer and the post-stimulus constants were adjusted to reflect the faster than expected return to the pre-stimulus state (Table S3). The two-, four-, and six-state kinetic models were solved using a python code. The set of first order differential equations were integrated with scipy.integrate.odeint.

Online supplemental material

Fig. S1 shows kinetic schemes used to simulate Hv1 mechanosensitive gating. Fig. S2 shows the proposed vicious cycle connecting brain damage to Hv1 hyperactivation in the microglia. Fig. S3 shows a schematic representation of two processes proposed to be involved in the facilitation of Hv1 activation by membrane stretch. Fig. S4 shows long-lasting facilitation observed in dimeric Hv1, which is proposed to be linked to changes in the dimer interface. Tables S1 and S2 show modeling of the application of tension at −20 mV and 80 mV, respectively, to the Hv1 dimer. Table S3 shows modeling of the application of tension at 80 mV to the Hv1 monomer.

RESULTS

Hv1 voltage-dependent activation is facilitated by membrane stretch

We recorded proton currents in inside-out membrane patches from *Xenopus* oocytes expressing wild-type human Hv1 in response to membrane depolarization and tested the effect of membrane stretch on the channel's activation and deactivation kinetics and voltage dependence of activation. To minimize changes in local proton concentration induced by Hv1 activity, we used a high concentration of pH buffer (100 mM) in both pipette and bath solutions and optimized channel density to have proton currents no bigger than 1 nA. The major charged species in all media were buffer ions, TEA, and methanesulfonate (see Materials and methods). Under these conditions, we did not observe activity of endogenous mechanosensitive channels. Changes in membrane stretch were achieved via HSPC connected to the patch pipette (Fig. 1, A and B). Currents were measured soon after membrane excision under no-pressure conditions (Fig. 1 B, black trace) and then again under a negative pressure step (Fig. 1 B, red trace). The magnitudes of the pressure pulses were in the range 10–25 mmHg, typically used to stimulate the opening of bona fide stretch-activated cation channels (Patel et al., 1998; Maingret et al., 1999; Maroto et al., 2005; Coste et al., 2010; Pathak et al., 2014). Negative pressure in the pipette in inside-out configuration corresponds to positive pressure inside the cell (i.e., pressure that would cause cell swelling). To quantify the effect of negative pressure stimulation, we performed monoexponential fits of the current traces (DeCoursey and Cherny, 1995) and used the single time constant (τ_a) as an approximate kinetic parameter. The effect on the deactivation kinetics parameter (τ_d) was quantified by monoexponential fitting of tail currents measured after a depolarization step (Fig. 1 C). Whereas activation kinetics showed strong acceleration (reduction in τ_a) in the presence of negative pressure (more than fourfold change at 60 mV; Fig. 1, B, D, and E), the effect on channel deactivation (τ_d) was not statistically significant (Fig. 1, C and E). The voltage dependence of channel activation was derived from tail currents as previously described (Tombola et al., 2010). Comparison of G-V curves measured in the absence and in the presence of negative pressure (Fig. 1 F) shows that membrane stretch produced a shift in the voltage of half-activation ($V_{1/2}$) of −14.4 ± 2.7 mV (activation requires less depolarized potentials) and a 32 ± 8% increase in the steepness of the curve (measured as a reduction in the slope factor *s*).

We wondered whether the observed effects of membrane stretch required a homodimerically assembled channel complex or could be attributed to mechanosensitive properties of the individual VSD subunit. To address this question, we examined the response to negative pressure stimulation of the $Hv1NC_{VSP}$ channel (Fig. 2 A), in which the Hv1 cytoplasmic N- and C-terminal domains are replaced by the corresponding parts of the voltage-sensitive phosphatase CiVSP (Murata et al., 2005; Kohout et al., 2008). $Hv1NC_{VSP}$ was previously found to be monomeric (Tombola et al., 2008). Hv1 constructs lacking the C-terminal CCD have faster gating kinetics and open at more depolarized voltages than the dimeric wild-type channel (Koch et al., 2008; Tombola et al., 2008). Activation in these constructs is well represented by a monoexponential curve (Fujiwara et al., 2013).

$Hv1NC_{VSP}$ activation was accelerated (τ_a decreased) by negative pressure stimulation (Fig. 2, A, B, D, and E) to an extent similar to what was observed with dimeric Hv1, whereas the kinetics of deactivation were not sensitive to the stimulus (Fig. 2, C and E). Negative pressure in the pipette shifted the voltage dependence of activation of $Hv1NC_{VSP}$ to less depolarized potentials

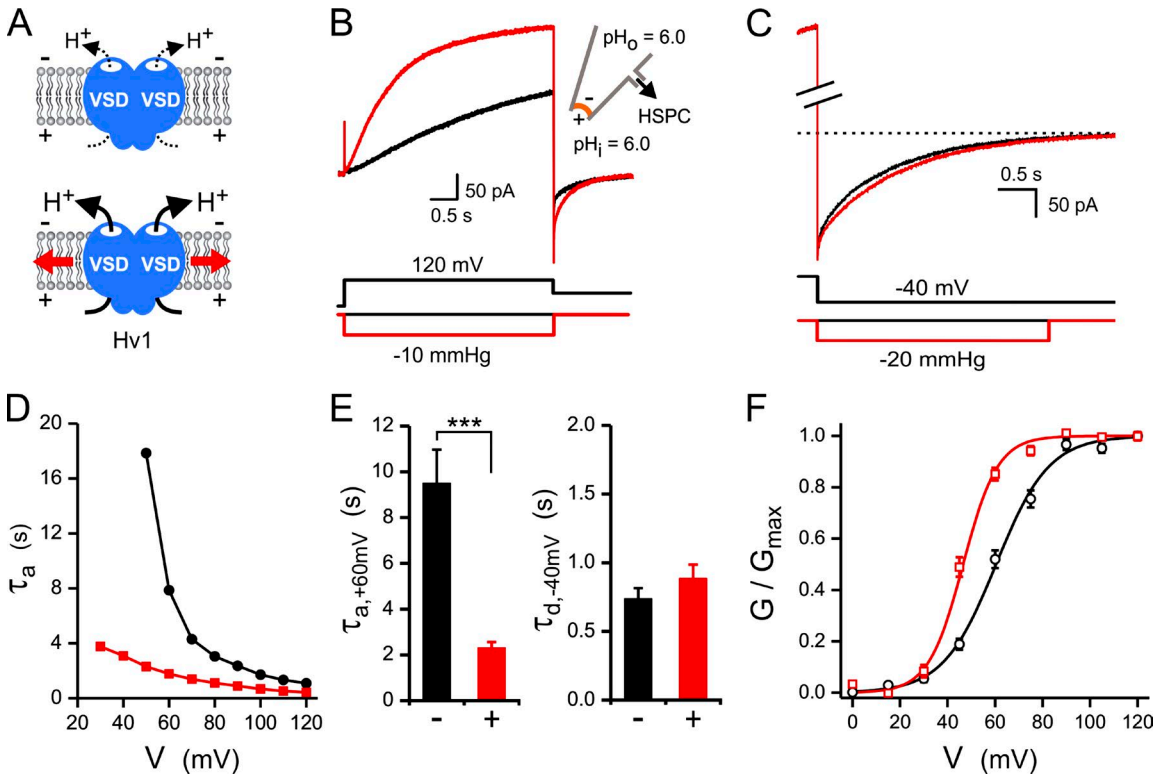

Figure 1. **Hv1 response to combined electrical and mechanical stimulation.** (A) Schematic representation of dimeric Hv1 stimulated by membrane stretch (red arrows). (B) Effect on Hv1 activation: Proton currents were measured in response to membrane depolarization in the absence (black) and presence (red) of negative pressure in the pipette. Holding potential: −80 mV, holding pressure: 0 mmHg. (C) Effect on Hv1 deactivation: Tail currents were measured at −40 mV after a depolarization pulse at 120 mV in the absence (black) and presence (red) of negative pressure in the pipette. Holding conditions and proton concentrations were as in B. Dotted line corresponds to 0 pA. Break in the current axis corresponds to 200 pA. (D) τ_a as a function of applied voltage without pressure stimulation (black circles) and in the presence of −10 mmHg pressure in the pipette (red squares). (E, left) Effect of −10-mmHg-pressure stimulation on τ_a measured at 60 mV; $n = 11$; ***, $P < 0.0001$. (right) Effect of −20-mmHg-pressure stimulation on τ_d measured at −40 mV; $n = 3$; $P > 0.05$. (F) Effect on G-V curve of negative pressure in the pipette. G-Vs measured at 0 mmHg and −10 mmHg are shown in black and red, respectively. Boltzmann fit parameters are $V_{1/2} = 60.5 \pm 1.5$ mV and $s = 11.0 \pm 0.8$ mV for the 0-mmHg condition ($n = 10$) and $V_{1/2} = 46.1 \pm 1.2$ mV and $s = 7.5 \pm 0.4$ mV for the −10-mmHg condition ($n = 10$). $P < 10^{-6}$ and $P < 0.002$ for differences in $V_{1/2}$ and s, respectively. Errors bars are SEM.

(Fig. 2 F), as observed with dimeric Hv1, but to a smaller extent: $\Delta V_{1/2} = -4.5 \pm 1.7$ mV. The steepness of the G-V curve did not increase with the pressure stimulus, but rather decreased 11 ± 4%.

Thus, Hv1 activation is facilitated by electrical and mechanical co-stimulation, and the most mechanosensitive parameter both in the monomeric and dimeric channel is the rate constant of channel activation (or its inverse, τ_a). For the rest of the study, we use this parameter as a readout of the channel's response to membrane stretch. The different effects of mechanical stimulation on the G-V curves of monomeric and dimeric Hv1 indicate that allosteric interactions between subunits can influence the intrinsic mechanosensitivity of the Hv1 VSD.

Short- and long-lasting effects of membrane stretch on Hv1 activation

To gain further insight on Hv1 mechanosensitivity, we examined the changes in proton current induced by pulses of negative pressure of short duration applied during channel activation by membrane depolarization (Fig. 3, A and C). If the only effect of mechanical stimulation was to reversibly increase the channel's activation rate, the proton current should increase more rapidly during the pressure pulse, and the excess of open channels thus generated should gradually decrease after termination of the pressure pulse to satisfy the steady-state conditions for the applied membrane potential at zero pressure. These features were evident in the proton currents during and after the pressure pulses (indicated by red and gray arrowheads in Fig. 3 [B and D], respectively), but two additional features revealed that the effect of membrane stretch on Hv1 had multiple components. One of the additional features was a fast (<10-ms time scale) increase in proton current at the onset of the pressure pulse, followed by a fast decrease in current coinciding with the termination of the pulse (Fig. 3, B and D, blue arrowheads). The extent of this fast component was small when the mechanical stimulus was applied at the

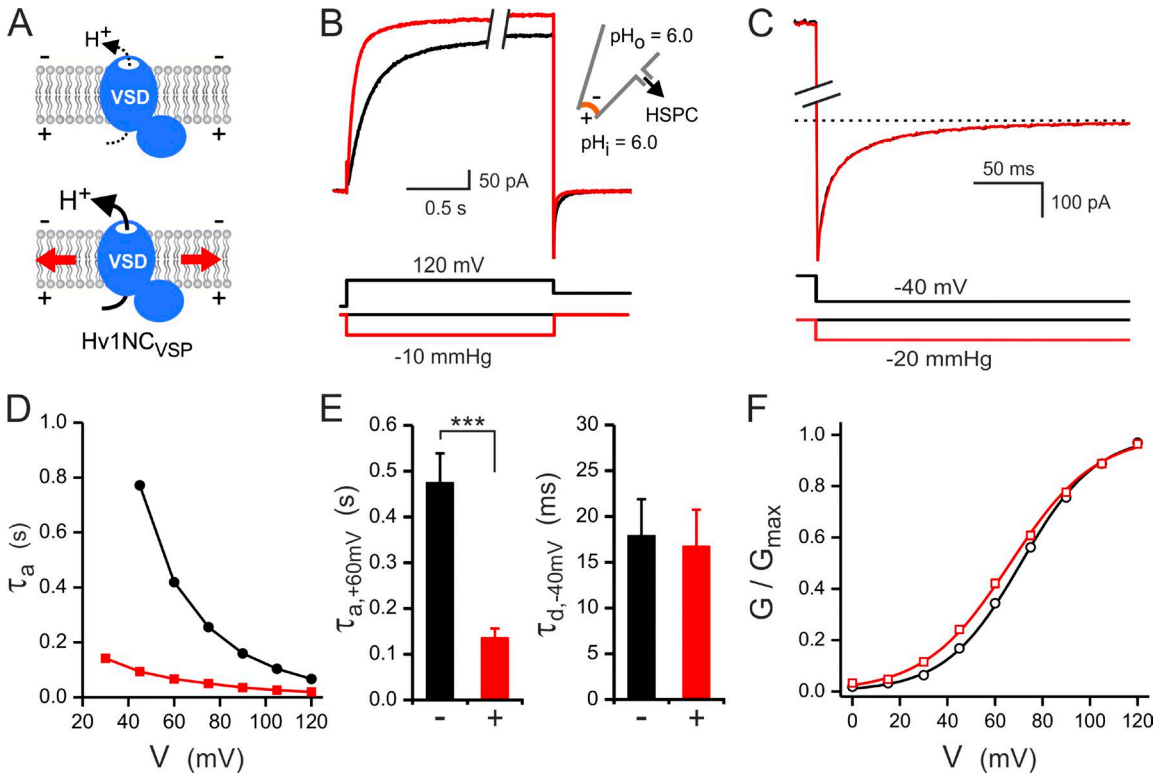

Figure 2. **Hv1NC$_{VSP}$ response to combined electrical and mechanical stimulation.** (A) Schematic representation of monomeric Hv1NC$_{VSP}$ stimulated by membrane stretch (red arrows). (B) Effect on Hv1NC$_{VSP}$ activation: Proton currents were measured in response to membrane depolarization in the absence (black) and presence (red) of negative pressure in the pipette. Holding potential: −80 mV, holding pressure: 0 mmHg. Break in the time axis corresponds to 1.5 s. (C) Effect on Hv1NC$_{VSP}$ deactivation: Tail currents were measured at −40 mV after a depolarization pulse at 120 mV in the absence (black) and presence (red) of negative pressure in the pipette. Holding conditions and proton concentrations were as in B. Dotted line corresponds to 0 pA. Break in the current axis corresponds to 650 pA. (D) τ_a values measured as a function of applied voltage without pressure stimulation (black circles) and in the presence of −10 mmHg pressure in the pipette (red squares). (E, left) Effect of −10-mmHg-pressure stimulation on τ_a measured at 60 mV; n = 14; ***, P < 0.0001. (right) Effect of −20-mmHg-pressure stimulation on τ_d measured at −40 mV; n = 5; P > 0.05. (F) Effect on G-V curve of negative pressure in the pipette. G-Vs measured at 0 mmHg and −10 mmHg are shown in black and red, respectively. Boltzmann fit parameters are $V_{1/2}$ = 70.9 ± 0.7 mV and s = 16.1 ± 0.4 mV for the 0-mmHg condition (n = 26) and $V_{1/2}$ = 66.4 ± 1.0 mV and s = 18.1 ± 0.4 mV for the −10-mmHg condition (n = 26). P < 0.001 and P < 0.002 for differences in $V_{1/2}$ and s, respectively. Errors bars are SEM. In F, error bars are smaller than symbols.

beginning of the depolarization step (Fig. 3, A and B) and became larger when the mechanical stimulus was applied later during the depolarization step (Fig. 3, C and D). Because the fraction of open channels increases over time during depolarization before reaching steady state, one possible explanation for the observed fast component is a stretch-induced conformational change that increases the conductance of the open channels. The other additional feature was the excess current remaining after termination of the mechanical stimulus (Fig. 3, A and C, black arrowheads). The current after the pressure pulse was consistently larger than the isochronal current expected at the end of the voltage step in the absence of the pressure pulse, suggesting that the effect of membrane stretch has a long-lasting component.

We then measured proton currents from Hv1NC$_{VSP}$ in response to pressure pulses of short duration (Fig. 4). We found that the fast components of the change in current (Fig. 4, B and D, blue arrowheads) were similar to those observed in the wild-type channel. The slower components (Fig. 4, B and D, red and gray arrowheads) were also similar. However, with Hv1NC$_{VSP}$, there was no excess current remaining after termination of the mechanical stimulus (Fig. 4, A and C, black arrowheads). The current after the pressure pulse was the same as the isochronal current expected at the end of the voltage step in the absence of the pressure pulse. This finding suggests that the long-lasting alteration induced by membrane stretch in wild-type Hv1 is either absent in Hv1NC$_{VSP}$ or quickly reversible.

We wondered whether the long-lasting alteration in wild-type Hv1 responsible for the excess current after mechanical stimulation could be revealed by consecutive membrane depolarizations and asked whether this alteration could occur when membrane stretch and membrane depolarization are not delivered simultane-

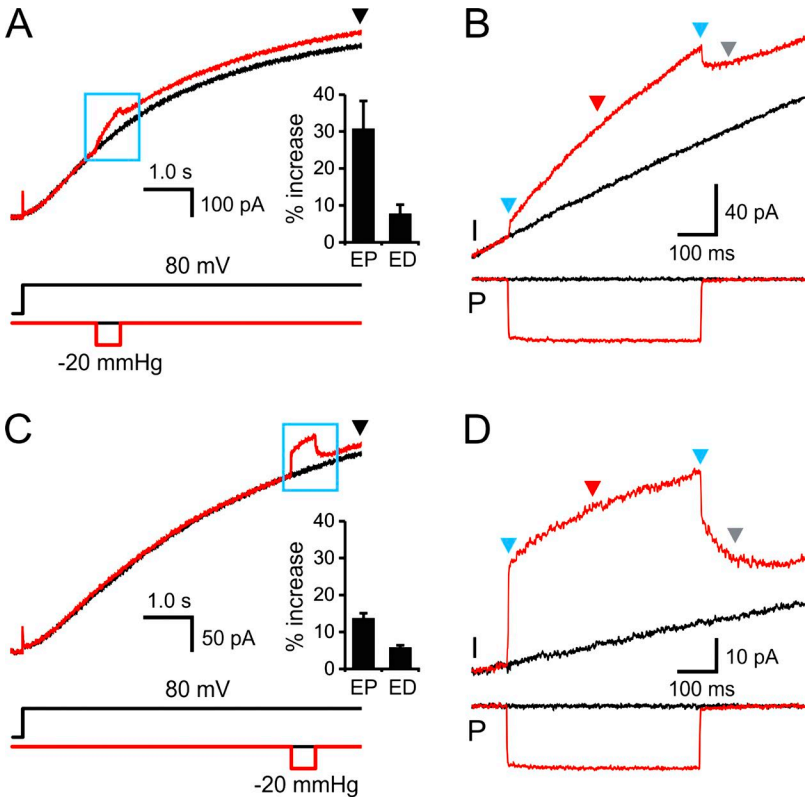

Figure 3. **Effects of brief mechanical stimulation on Hv1 activation.** (A) Hv1 current was elicited by membrane depolarization as in Fig. 1 B and measured in the absence of mechanical stimulation (black) and in the presence of a brief pulse of negative pressure in the pipette (red). The pulse was delivered when the fraction of open channels generated by voltage-dependent activation was still small. See Materials and methods for details. (B) Enlarged view of current traces (I) enclosed in the blue square in A. Pressure traces recorded during stimulation are also shown (P). (C) Hv1 currents were measured as in A, but with the mechanical stimulus delivered when voltage-dependent activation had produced a larger fraction of open channels. (A and C) Inset bar charts indicate the mean relative increase in current measured at the end of the pulse (EP) and the mean residual increase in current measured at the end of the depolarization step (ED). Error bars are SEM (n = 5). (D) Enlarged view of current traces (I) enclosed in the blue square in C and corresponding pressure traces (P). Black arrowheads in A and C indicate difference in isochronal current at the end of the two traces (ED > 0). Red, blue, and gray arrowheads in B and D indicate different components of the effect of mechanical stimulation on Hv1 activation.

ously. We interrogated Hv1 with a protocol consisting of two consecutive voltage steps separated by a fixed interval during which a pressure pulse was applied with or without a simultaneous voltage step (Fig. 5, A–D). To quantify changes in activation kinetics between the "T" depolarization (test) and the "R" depolarization (reference), we calculated the ratio $\tau_{a,T}/\tau_{a,R}$. We found that this ratio significantly decreased when a pressure pulse was applied between the two voltage steps (Fig. 5 E, $P < 0.0001$), indicating that membrane stretch causes an acceleration of channel activation that persists in the absence of the pressure pulse. In addition, we found that electrical co-stimulation is not required to achieve membrane stretch–induced facilitation of channel activation (Fig. 5 E).

When Hv1 was stimulated with three consecutive depolarizations (R, P, and T), as shown in Fig. 5 (D and F), the pressure pulse delivered with the second depolarization induced faster channel activation during the third depolarization as compared with the first depolarization ($\tau_{a,T} < \tau_{a,R}$, $P < 0.0001$). Remarkably though, channel activation elicited by the third pulse (T) was also faster than the activation elicited by combined electrical and mechanical stimulation (second pulse [P]; $\tau_{a,T} < \tau_{a,P} < \tau_{a,R}$; Fig. 5 F, purple open diamonds; $P < 0.001$). The simplest explanation for this hysteretic behavior is that when the channel closes at the end of the second depolarization, it does not go back to the original closed state, but to a nonconducting facilitated state from which it is easier to transition to the open state.

We asked whether the facilitated state would slowly revert to the normal closed state in the absence of mechanical stimulation. We applied the double three-pulse protocol shown in Fig. 5 F in which the first set of pulses (control) is used to induce facilitation, and the second set is used to assess the recovery from the facilitated state after a time interval Δt. Facilitation was estimated as an acceleration of channel activation during the second and third depolarizations compared with the first depolarization (reduction in normalized τ_a within each set of pulses). With the shortest interval (Δt = 1 s; Fig. 5 F, left, light gray filled circles), the recovery of facilitation was partial, as mechanical stimulation could still accelerate activation in the second pulse ($\tau_{a,P} < \tau_{a,R}$, $P < 0.001$), but no further acceleration was observed in the third pulse ($\tau_{a,T} \approx \tau_{a,P}$, $P > 0.05$). Similar results were obtained with a Δt of 60 s (Fig. 5 F, left, gray filled squares). To observe full recovery of facilitation, an extension of Δt to 300 s was required (Fig. 5 F, left, black filled diamonds and control purple open diamonds almost superimposable).

The finding that facilitation within individual sets of pulses can be completely recovered after 300 s suggests that the effect of mechanical stimulation on channel activity is fully reversible. If this were the case, we would also expect $\tau_{a,R}$ to completely recover within 300 s to its original value ($\tau_{a,R(\Delta t = 300\ s)}/\tau_{a,R(Control)} = 1$). So we measured the ratio $\tau_{a,R(\Delta t)}/\tau_{a,R(Control)}$ at Δt = 1, 60, and 300 s (Fig. 5 F, right, black columns) and compared it with the value expected for complete recovery (Fig. 5 F,

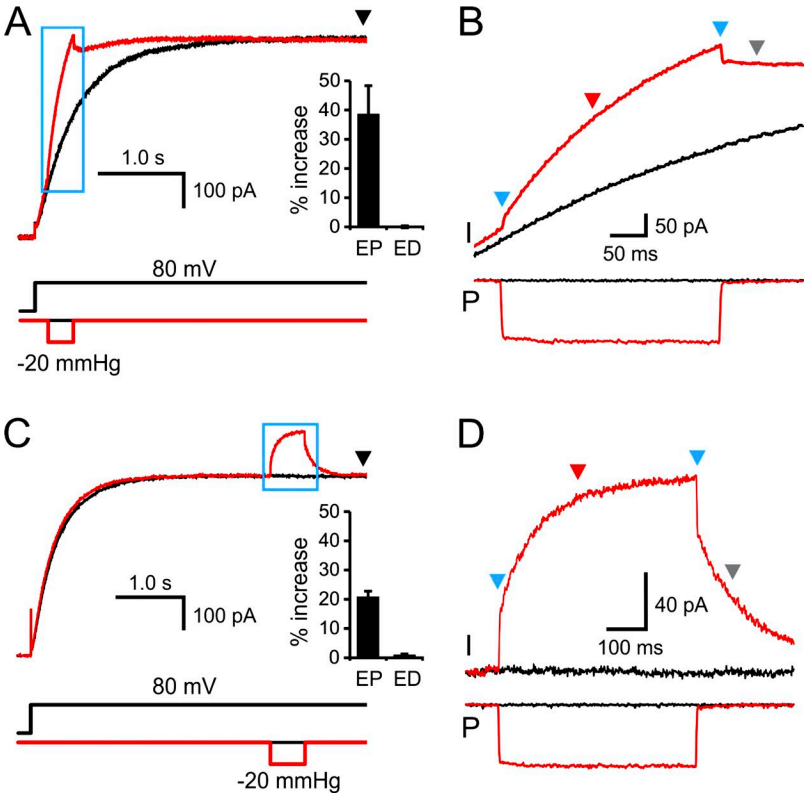

Figure 4. **Effects of brief mechanical stimulation on Hv1NC$_{VSP}$ activation.** (A) Hv1NC$_{VSP}$ current was elicited by membrane depolarization as in Fig. 2 B and measured in the absence of mechanical stimulation (black) and in the presence of a brief pulse of negative pressure in the pipette (red). The pulse was delivered when the fraction of open channels generated by voltage-dependent activation was still small. See Materials and methods for details. (B) Enlarged view of current traces (I) enclosed in the blue rectangle in A. Pressure traces recorded during stimulation are also shown (P). (C) Hv1 currents were measured as in A, but with the mechanical stimulus delivered when voltage-dependent activation had produced a larger fraction of open channels. (A and C) Inset bar chart indicates the mean relative increase in current measured at the end of the pulse (EP) and the mean residual increase in current measured at the end of the depolarization step (ED). Error bars are SEM (n = 5). (D) Enlarged view of current traces (I) enclosed in the blue square in C and corresponding pressure traces (P). There was no difference in isochronal current at the end of the two traces in A and C (black arrowheads, ED ≈ 0). Red, blue, and gray arrowheads in B and D indicate different components of the effect of mechanical stimulation on Hv1 activation.

right, purple columns). At the shorter Δts, channel activation was still faster than the control ($\tau_{a,R(\Delta t)}/\tau_{a,R(Control)} < 1$, $P < 0.01$), indicating that the accelerating effect of the mechanical stimulation had not yet reversed. In contrast, at $\Delta t = 300$ s, channel activation was no longer accelerated ($\tau_{a,R(\Delta t = 300\ s)}/\tau_{a,R(Control)} \geq 1$; Fig. 5 F, right). Although the $\tau_{a,R(\Delta t = 300\ s)}/\tau_{a,R(Control)}$ ratio was not significantly higher than 1 ($P > 0.05$), we cannot rule out the possibility of an additional process that slows down channel activation after the accelerating effect of mechanical stimulation has subsided. Nonetheless, based on these results and the complete recovery from facilitation within individual set of pulses reported above, it is reasonable to conclude that the effect of membrane stretch on Hv1 activation is reversible.

Together, these measurements show that the mechanical stimulus causes dimeric Hv1 to accelerate its voltage-dependent activation and to switch to a facilitated state from which the channel can open more easily. Switching to the facilitated state does not require membrane depolarization, and the channel can stay facilitated for minutes after the mechanical stimulus is terminated. The mechanical stimulus causes similar effects in monomeric Hv1 (Figs. 2 and 4). But, in the monomeric form, the channel can return to the nonfacilitated state more rapidly, as indicated by the lack of poststimulation current enhancement in Fig. 4 (A and C).

The fast on and off kinetics of the proton current in response to brief pressure pulses and the minimal delays between the changes in pressure and the changes in current (Figs. 3 and 4) indicate that the slack in the system is negligible. We cannot completely exclude that the long-lasting facilitation observed in dimeric Hv1 is caused by residual membrane tension persisting after the termination of the pressure pulse. However, the fact that we do not observe poststimulation current enhancement in monomeric Hv1 (Fig. 4) is more consistent with facilitation being a property of the channel rather than the membrane.

Hv1 activation by membrane stretch in the presence of a transmembrane pH gradient

Hv1 requires strong and sustained depolarizations to open in the absence of a transmembrane pH gradient. The $V_{1/2}$ of the activation curve has been reported to be between 50 and 65 mV when $\Delta pH_m = pH_o - pH_i = 0$ (Ramsey et al., 2006; Sasaki et al., 2006; Tombola et al., 2008). However, the channel is known to open at less depolarized potentials when the intracellular pH is lower than the extracellular pH ($\Delta pH_m > 0$; Cherny et al., 1995; Ramsey et al., 2006; Sasaki et al., 2006; Villalba-Galea, 2014). Because we found that membrane stretch can facilitate Hv1 activation even in the absence of membrane depolarization, we asked whether mechanical stimulation alone could result in channel opening in the presence of a favorable ΔpH_m. To test for this possibility, we recorded Hv1 currents from inside-out patches exposed to intracellular and extracellular solutions of different pH (pH_i 6.0 and pH_o 7.5; Fig. 6). The

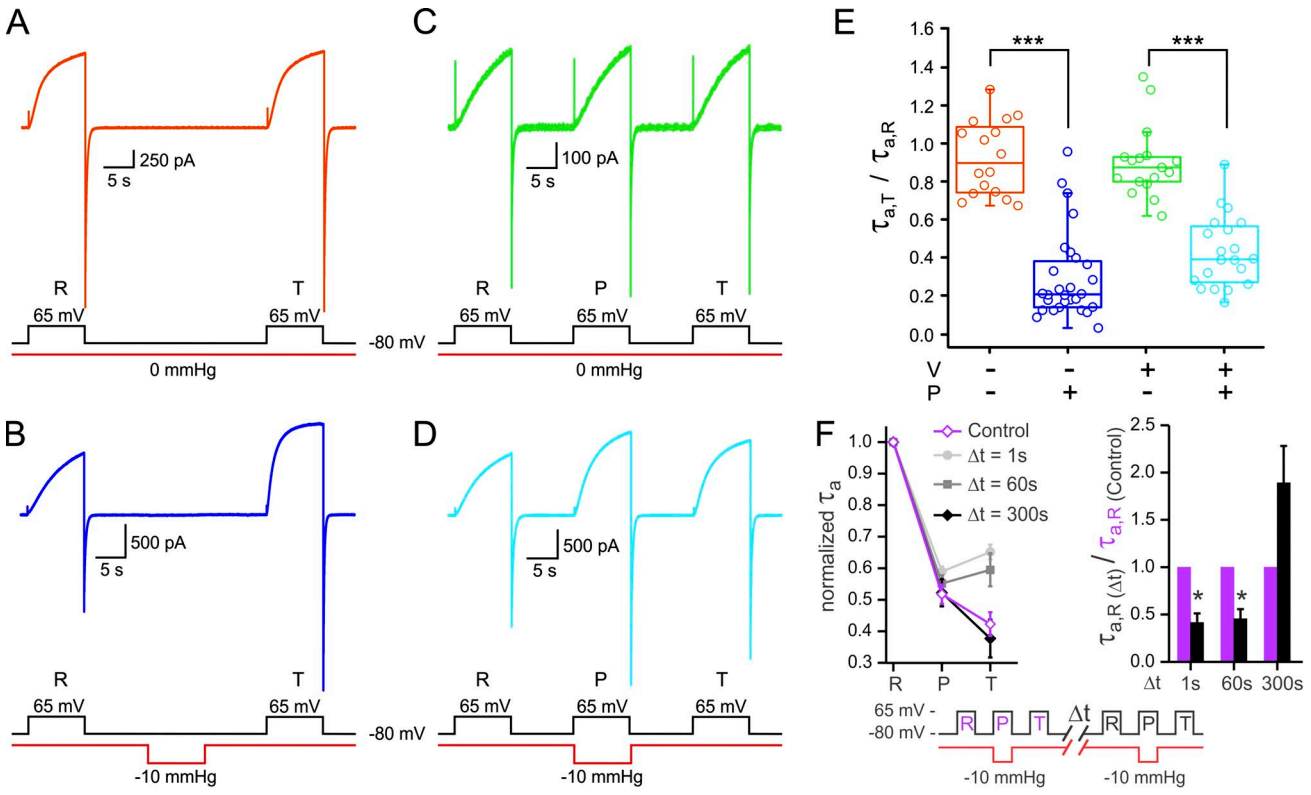

Figure 5. **Long-lasting effect of membrane stretch on Hv1 activation does not require membrane depolarization and is slowly reversible.** (A) Hv1 proton current elicited by consecutive depolarization steps R (reference) and T (test) in the absence of mechanical stimulation (pH_i and pH_o 6.0). Changes in kinetics of activation between the first and second depolarization are quantified by the ratio $\tau_{a,T}/\tau_{a,R}$ reported in E. (B) Hv1 current measured as in A with mechanical stimulation (negative pressure) delivered at holding membrane potential between T and R pulses. (C) Hv1 current measured as in A with an additional depolarization step (P) between the reference and test pulses. (D) Hv1 current measured as in C with mechanical stimulation delivered during the depolarization step (P) between T and R pulses. (E) Box plot comparing $\tau_{a,T}/\tau_{a,R}$ values measured under the voltage and pressure protocols shown in A–D. $\tau_{a,T}/\tau_{a,R} < 1$ indicates accelerated activation kinetics during the T pulse compared with the R pulse. Boxes indicate median ± SD. Whiskers show 5th and 95th percentiles. Asterisks indicate statistically significant difference: ***, $P < 0.0001$. (F) Recovery from membrane stretch–induced acceleration of Hv1 activation. Hv1 was first activated with a combined voltage/pressure protocol as in D. (left) $\tau_{a,R}$, $\tau_{a,P}$, and $\tau_{a,T}$ parameters were measured and normalized, using $\tau_{a,R}$ as reference. After the time interval Δt, the combined voltage/pressure protocol was applied again, and the normalized τ_a values were recalculated. The protocol was applied only once per patch. Light gray circles (Δt = 1 s): $n = 4$. Gray squares (Δt = 60 s): $n = 5$. Black diamonds (Δt = 300 s): $n = 7$. Error bars are SEM. (right) Bar chart showing the recovery of $\tau_{a,R}$ over time after mechanical stimulation (black columns). The reference values corresponding to full recovery are shown as purple columns. Error bars are SEM. Asterisks indicate statistically significant difference: *, $P < 0.01$. The normalized $\tau_{a,P}$ and $\tau_{a,T}$ values in the left panel corresponding to a particular Δt ($\tau_{a,P}(\Delta t)/\tau_{a,R}(\Delta t)$, and $\tau_{a,T}(\Delta t)/\tau_{a,R}(\Delta t)$) can be renormalized relative to $\tau_{a,R}$(control) using the corresponding $\tau_{a,R}(\Delta t)/\tau_{a,R}$(control) ratios from the right panel as multiplication factors.

membrane potential was maintained to a negative value (−30 to −20 mV), close to the channel activation threshold. Under these conditions, the channel was closed (Fig. 6 B, black trace), but opened upon stimulation with a pressure pulse (Fig. 6, B [red trace] and C). The complete absence of stretch-induced currents in noninjected cells (Fig. 6 C, NI) indicates that measured currents are from Hv1 and not from endogenous stretch-activated channels.

Models of Hv1 mechanosensitivity

We then set out to determine the simplest kinetic model that could reproduce the main features of Hv1 mechanosensitive activation. We started with a basic two-state scheme (C ↔ O; Fig. S1) in which the forward and backward rates are modulated by membrane tension such that their g(V) curve would hyperpolarize with elevated membrane tension, as per Fig. 1 F. This aspect is essentially as for Kv channels with a mechanosensitive V-dependent transition (Morris et al., 2015). The model was able to mimic the increase in Hv1-mediated proton conductance elicited by pulses of negative pressure delivered at membrane potentials close to the activation threshold (Figs. 6 and 7 A) but could not reproduce the more complex features observed when Hv1 was exposed to short mechanical stimuli in the presence of stronger membrane depolarization (Figs. 3 and 7 C). Thus, we added a second tension-modulated V-dependent closed-open pair ($C_p \leftrightarrow O_p$) to the basic scheme (Fig. S1). In the resulting four-state model, the mechanical stimulus

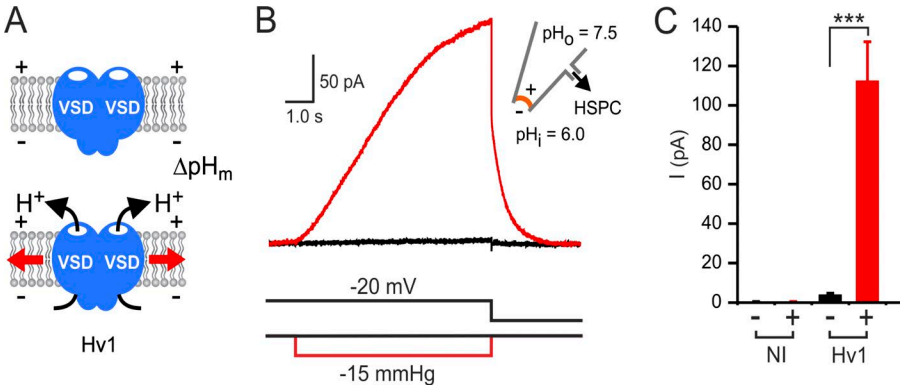

Figure 6. **Hv1 response to mechanical stimulation in the presence of a pH gradient.** (A) Schematic representation of dimeric Hv1 opened by membrane stretch (red arrows) when $\Delta pH_m = pH_o - pH_i > 0$. (B) Proton currents were recorded at a membrane potential sufficiently negative to prevent voltage-dependent channel activation in the absence of mechanical stimulation (between −30 and −20 mV; black). The current was then recorded again at the same voltage but in the presence of negative pressure in the pipette (red). At the end of the pressure step, the voltage was changed to −80 mV. (C) Quantification of the proton current elicited by negative pressure stimulation under conditions described in B. Membrane patches from noninjected cells (NI) displayed no stretch-induced currents. Error bars are SEM (n = 5 for NI, n = 11 for Hv1). Asterisks indicate statistically significant difference: ***, P < 0.0001.

affects the C ↔ O transition as in the two-state model, but also facilitates access to conformations C_p and O_p. The conductance of the O_p state is ∼25% larger than the conductance of the O state to allow for the sharp increase and decrease in total proton conductance when the mechanical stimulus is turned on and off, respectively (Fig. 3, B and D, blue arrowheads; and Fig. 7 C). For simplicity, the rates of the $C_p \leftrightarrow O_p$ transition were set to be the same as for the C ↔ O transition, and the mechanical stimulus was assumed to affect the two transitions to the same extent. In addition, the forward and backward rates in the fast $C \leftrightarrow C_p$ and $O \leftrightarrow O_p$ transitions were chosen to be equal, explaining why O and O_p rise together in Fig. 7 B. The four-state model was able to replicate all of the short-lasting effects of mechanical stimulation on dimeric and monomeric Hv1 (Figs. 3, 4, and 7, C and D; and Tables S1 and S3).

The long-lasting increase in proton conductance observed after mechanical stimulation of Hv1 wild type (Fig. 3, A and C, black arrowheads) could not be properly simulated with the four-state model (Fig. 7 C, black curve). Hence, we added a third tension-modulated V-dependent closed-open pair ($C_{pp} \leftrightarrow O_{pp}$), increasing the total number of states to six (unitary conductance of O_{pp} same as O_p). The mechanical stimulus was assumed to increase the $C_{pp} \rightarrow O_{pp}$ rate twice as much as the $C \rightarrow O$ and $C_p \rightarrow O_p$ rates. The transitions connecting C_{pp} to C_p and O_{pp} to O_p were set to become very slow (rates ≈ 0) in the absence of the mechanical stimulus. This restraint, in combination with a poststimulus deceleration of the $C_p \rightarrow C$ and $O_p \rightarrow O$ transitions (Table S2) led to an accurate simulation of the long-lasting Hv1 facilitation induced by membrane tension (Fig. 7 C, purple curve).

This approach of stepwise increasing modeling complexity allows us to conclude that the four- and six-state models are the simplest models that accurately simulate the observed effects of mechanical stimulation on monomeric and dimeric Hv1, respectively. A possible structural interpretation for the requirement of two extra states for the dimer is reported in the Discussion.

DISCUSSION

Hv1 is expressed in cells that do not normally change their membrane potential to the extent required to fully activate the whole channel population, especially in the absence of a favorable transmembrane pH gradient. Although Hv1 can experience favorable ΔpH_m in phagocytes during the respiratory burst (DeCoursey, 2013), similarly favorable conditions are unlikely to occur in other cells, where homeostatic mechanisms prevent substantial intracellular acidification, e.g., B lymphocytes (Marches et al., 2001; Capasso et al., 2010) and basophils (Musset et al., 2008), or where the intracellular pH can be higher than the extracellular pH, e.g., osteoclasts (Nordström et al., 1995; Mori et al., 2003) and sperm cells (Lishko et al., 2010; O'Hanlon et al., 2013). As a result, it is unlikely that the channel's full activation can be produced by membrane depolarization alone under physiological conditions.

Besides ΔpH_m, little is known about the physical or chemical factors that modulate Hv1 gating. Changes in temperature are known to affect Hv1 activation (DeCoursey and Cherny, 1998; Kuno et al., 2009; Fujiwara and Okamura, 2014), and protein modifications, such as phosphorylation (Morgan et al., 2007; Musset et al., 2010a), or alternative protein initiation (Hondares et al., 2014) can produce Hv1 channels with faster activation kinetics. However, these stimuli operate on a time scale different than voltage gating and are not specific to membrane compartments exposed to mechanical forces.

Facilitation of Hv1 activation by membrane stretch occurs within the time scale of voltage gating and allows the channel to rapidly open under the moderate depolarization conditions typically found in cellular compartments physiologically exposed to mechanical forces, such as the apical membrane of airway epithelial cells and the tail of

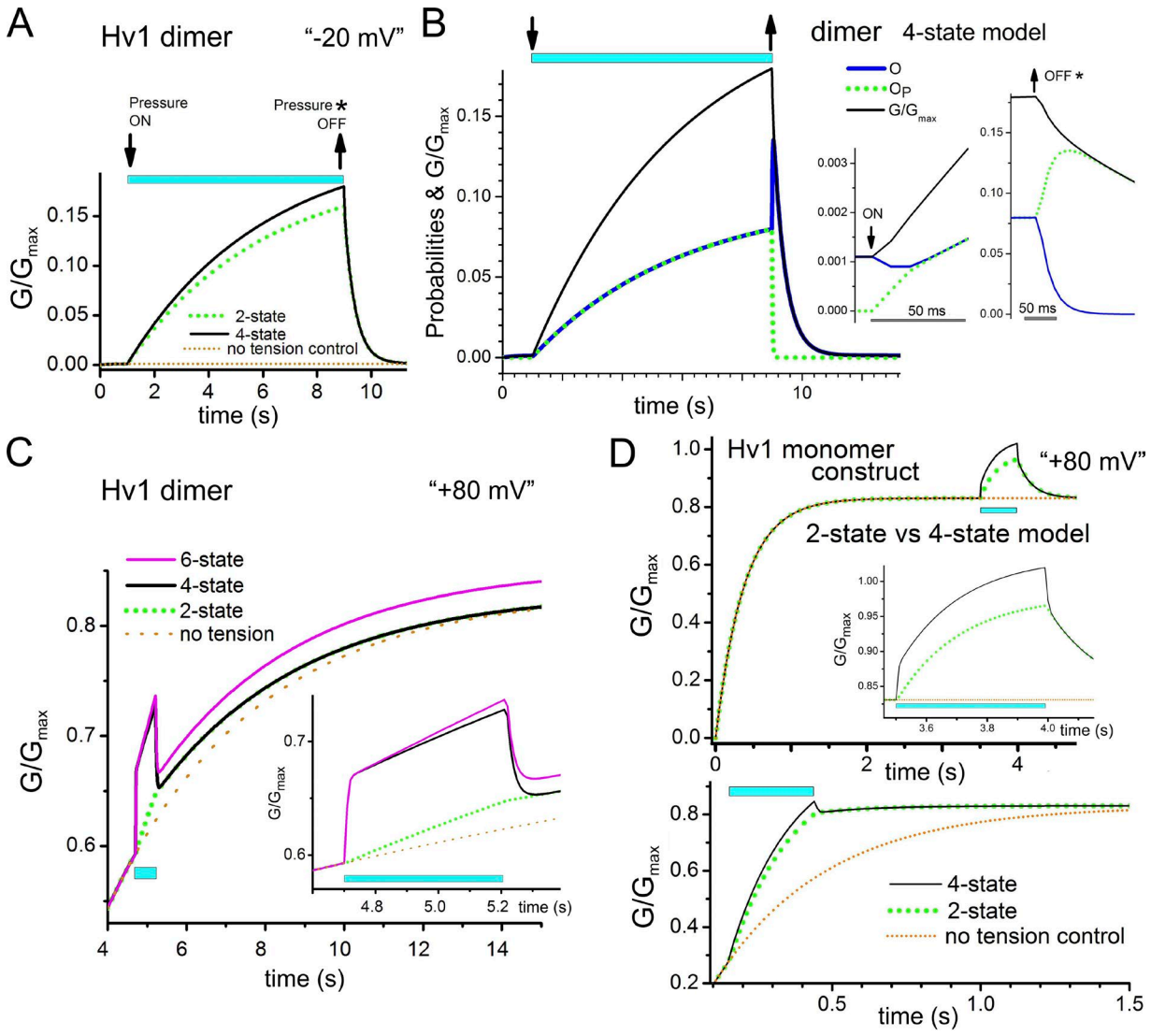

Figure 7. **Modeling mechanosensitive responses of Hv1 proton channels via two-, four-, or six-state kinetic schemes.** Simulations of time courses of normalized proton conductance ($G/G_{max}(t)$) in response to increase in membrane tension for dimeric (A–C) and monomeric Hv1 (D). The kinetic schemes used for the simulations are shown in Fig. S1. Parameter values are in Tables S1, S2, and S3. Note that dimer kinetics are ∼10 times slower than monomer kinetics. (A and B) Simulation of Hv1 WT at V_m near the foot of its G-V curve ("−20 mV", see Fig. 6). B shows how the O (blue) and O_p (green) states contribute to the total conductance in the four-state model. Insets show the changes in state probabilities at the onset and offset of the pressure pulse. (C) Simulation of Hv1 dimer at V_m near the top of the G/V curve ("+80 mV"; see data traces in Fig. 3). Inset shows an enlarged view of the currents predicted by the three models during the pressure pulse. (D) Simulation of $Hv1NC_{VSP}$ at V_m = 80 mV (see data traces in Fig. 4). Inset in the top panel shows an enlarged view of the currents predicted by the two- and four-state models during the pressure pulse. Instantaneous onset and offset of increased membrane tension (in response, experimentally, to applied pipette aspiration, i.e., "Pressure on") is assumed. Asterisks in A and B indicate a step to V_{hold} simultaneous with Pressure off, as in some experiments.

sperm cells. In cases where Hv1 activation is already primed by other stimuli (e.g., ΔpH_m), additional stimulation by membrane stretch can render the channel hyperactive. Proton currents measured in microglial cells under conditions mimicking neuronal damage were previously found to be potentiated by cell swelling induced by intracellular acidosis or hypotonic stress (Morihata et al., 2000). Stroke-induced brain damage is associated with cell swelling (Mongin, 2007; Song and Yu, 2014) and acidosis (Siesjö et al., 1996; Xiong et al., 2004), and proton channel activation in the microglia was found to increase neuronal death in a mouse model of ischemic stroke (Wu et al., 2012). When microglial cells are exposed to acidosis, the ensuing cell swelling may cause the plasma membrane to stretch, at least transiently, triggering Hv1 transition to the facilitated gating mode. Microglia cells could use this mechanism to increase proton extrusion and counteract intracellular acidification (Morihata et al., 2000). However, Hv1 hyperactivation would also increase the production of toxic ROS (Wu et

al., 2012), as a result of the electrochemical coupling between the channel and NOX, ultimately leading to enhanced neuronal death (Fig. S2).

Voltage-gated potassium and sodium channels are known to be sensitive to mechanical stimulation, as their activation by membrane depolarization is modulated by membrane stretch (Laitko et al., 2006; Beyder et al., 2010; Schmidt et al., 2012; Hao et al., 2013). However, whether the effect of membrane stretch is mediated by their four VSDs or their pore domain is a subject of debate (Tabarean and Morris, 2002; Schmidt et al., 2012; Morris et al., 2015). Because the Hv1 channel lacks the pore domain and has a dimeric, rather than tetrameric, structural organization, it represents a simpler model to study how mechanical forces affect VSDs. Here, we find that the Hv1 VSD is intrinsically sensitive to membrane stretch, and that the allosteric coupling between the two VSD subunits modulates the effect of the mechanical stimulus on voltage-dependent activation. We also find that the effect has multiple components, some of which revert quickly, whereas others revert slowly and possibly not completely. As a result, the rate of channel activation by membrane depolarization depends on whether the channel has been previously exposed to membrane stretch, a hallmark of mechanical hysteresis.

A previous study on bacterial stretch-activated ion channels proposed that wetting and dewetting of a hydrophobic region in the permeation pathway can play a major role in defining the thermodynamics and kinetics of mechanosensitive channel gating and can be the origin of hysteretic behavior (Anishkin et al., 2010). The hydration/wetting of the core of the Hv1 VSD appears to be an important requirement for proton conduction (Freites et al., 2006; Ramsey et al., 2010; Wood et al., 2012), and water penetration into the core of the channel's transmembrane module is believed to change considerably upon channel opening (Chamberlin et al., 2014, 2015; Hong et al., 2014), especially in the proximity of the VSD charge transfer center or hydrophobic plug (Tao et al., 2010; Lacroix et al., 2014; Takeshita et al., 2014). So one possible origin for Hv1 mechanosensitivity could reside in changes of VSD wettability induced by membrane stretch, which would result in changes in the thermodynamic and kinetic properties of voltage-dependent gating (Fig. S3 A). Voltage-dependent opening in Hv1 has been proposed to involve conformational changes in the intracellular portion of the VSD, leading to an expansion of the intracellular vestibule (Hong et al., 2013; Mony et al., 2015). Thus, another possible source of mechanosensitivity could derive from alterations in protein–lipid interactions in the proximity of the intracellular vestibule. Membrane stretch could cause a stabilization of the expanded vestibule resulting in a facilitation of channel opening (Fig. S3 B).

The difference in long-lasting facilitation observed in dimeric versus monomeric channels can be explained by a distinct tension-dependent transition in the dimer complex, corresponding to the $C_{pp} \leftrightarrow O_{pp}$ transition in our model (Fig. S1). The simplest interpretation for this additional transition is a tension-dependent alteration of the dimer interface that cannot occur in the monomer (Fig. S4). The two Hv1 subunits are held together at the cytoplasmic CCD (Koch et al., 2008; Lee et al., 2008; Tombola et al., 2008; Li et al., 2010; Fujiwara et al., 2012), but they also interact inside the membrane (Li et al., 2015). The transmembrane VSD–VSD interface is more likely to be sensitive to membrane stretch than the CCD. The S4 helices of the two subunits were previously found to be part of the VSD–VSD interface and to form a continuous structural unit with the CCD (Fujiwara et al., 2014). The outer ends of the S1 segments were also found to participate in the dimer interface (Lee et al., 2008; Qiu et al., 2013; Hong et al., 2015), suggesting that the S4–S4 unit partially unwinds toward the extracellular side of the membrane (Hong et al., 2015). Membrane stretch could change the extent of this unwinding, consequently affecting the S4 movement associated with gating. Further studies will be necessary to test this possibility and other tension-induced changes in dimer interface. Nonetheless, the kinetic characteristics of the C_{pp} and O_{pp} states (Table S2) suggest that, in the absence of a mechanical stimulus, the dimer interfaces interconvert at a rate that is more than one order of magnitude slower than voltage gating (Fig. S4).

In conclusion, our finding that mechanical stimulation significantly enhances Hv1 activity by acting on the channel's VSDs provides a simple explanation for the phenomenon of proton current potentiation observed in the microglia after cell swelling induced by intracellular acidosis or hypotonic stress (Morihata et al., 2000). We thus propose that membrane stretch is one of the co-stimuli required to open Hv1 under the moderate depolarization conditions typically found in nonexcitable cells.

ACKNOWLEDGMENTS

We thank Stephen White for comments on the manuscript.

This work was supported by National Institutes of Health grants GM098973 and NS085628 and University of California, Irvine's Council on Research Computing and Libraries (CORCL) grant (to F. Tombola). B. Joós acknowledges support from the Natural Sciences and Engineering Research Council of Canada and C.E. Morris from the Ottawa Hospital Research Institute. T. Tran was supported in part by the Undergraduate Research Opportunities Program of the University of California, Irvine.

The authors declare no competing financial interests.

Richard W. Aldrich served as editor.

Submitted: 20 July 2016
Accepted: 22 September 2016

REFERENCES

Anishkin, A., B. Akitake, K. Kamaraju, C.S. Chiang, and S. Sukharev. 2010. Hydration properties of mechanosensitive channel pores

define the energetics of gating. *J. Phys. Condens. Matter.* 22:454120. http://dx.doi.org/10.1088/0953-8984/22/45/454120

Beyder, A., J.L. Rae, C. Bernard, P.R. Strege, F. Sachs, and G. Farrugia. 2010. Mechanosensitivity of Nav1.5, a voltage-sensitive sodium channel. *J. Physiol.* 588:4969–4985. http://dx.doi.org/10.1113/jphysiol.2010.199034

Capasso, M., M.K. Bhamrah, T. Henley, R.S. Boyd, C. Langlais, K. Cain, D. Dinsdale, K. Pulford, M. Khan, B. Musset, et al. 2010. HVCN1 modulates BCR signal strength via regulation of BCR-dependent generation of reactive oxygen species. *Nat. Immunol.* 11:265–272. http://dx.doi.org/10.1038/ni.1843

Chamberlin, A., F. Qiu, S. Rebolledo, Y. Wang, S.Y. Noskov, and H.P. Larsson. 2014. Hydrophobic plug functions as a gate in voltage-gated proton channels. *Proc. Natl. Acad. Sci. USA.* 111:E273–E282. http://dx.doi.org/10.1073/pnas.1318018111

Chamberlin, A., F. Qiu, Y. Wang, S.Y. Noskov, and H.P. Larsson. 2015. Mapping the gating and permeation pathways in the voltage-gated proton channel Hv1. *J. Mol. Biol.* 427:131–145. http://dx.doi.org/10.1016/j.jmb.2014.11.018

Cherny, V.V., V.S. Markin, and T.E. DeCoursey. 1995. The voltage-activated hydrogen ion conductance in rat alveolar epithelial cells is determined by the pH gradient. *J. Gen. Physiol.* 105:861–896. http://dx.doi.org/10.1085/jgp.105.6.861

Coste, B., J. Mathur, M. Schmidt, T.J. Earley, S. Ranade, M.J. Petrus, A.E. Dubin, and A. Patapoutian. 2010. Piezo1 and Piezo2 are essential components of distinct mechanically activated cation channels. *Science.* 330:55–60. http://dx.doi.org/10.1126/science.1193270

DeCoursey, T.E. 2013. Voltage-gated proton channels: molecular biology, physiology, and pathophysiology of the H_V family. *Physiol. Rev.* 93:599–652. http://dx.doi.org/10.1152/physrev.00011.2012

DeCoursey, T.E., and V.V. Cherny. 1995. Voltage-activated proton currents in membrane patches of rat alveolar epithelial cells. *J. Physiol.* 489:299–307. http://dx.doi.org/10.1113/jphysiol.1995.sp021051

DeCoursey, T.E., and V.V. Cherny. 1998. Temperature dependence of voltage-gated H^+ currents in human neutrophils, rat alveolar epithelial cells, and mammalian phagocytes. *J. Gen. Physiol.* 112:503–522. http://dx.doi.org/10.1085/jgp.112.4.503

Freites, J.A., D.J. Tobias, and S.H. White. 2006. A voltage-sensor water pore. *Biophys. J.* 91:L90–L92. http://dx.doi.org/10.1529/biophysj.106.096065

Fujiwara, Y., and Y. Okamura. 2014. Temperature-sensitive gating of voltage-gated proton channels. *Curr. Top. Membr.* 74:259–292. http://dx.doi.org/10.1016/B978-0-12-800181-3.00010-5

Fujiwara, Y., T. Kurokawa, K. Takeshita, M. Kobayashi, Y. Okochi, A. Nakagawa, and Y. Okamura. 2012. The cytoplasmic coiled-coil mediates cooperative gating temperature sensitivity in the voltage-gated H^+ channel Hv1. *Nat. Commun.* 3:816. http://dx.doi.org/10.1038/ncomms1823

Fujiwara, Y., T. Kurokawa, K. Takeshita, A. Nakagawa, H.P. Larsson, and Y. Okamura. 2013. Gating of the designed trimeric/tetrameric voltage-gated H^+ channel. *J. Physiol.* 591:627–640. http://dx.doi.org/10.1113/jphysiol.2012.243006

Fujiwara, Y., T. Kurokawa, and Y. Okamura. 2014. Long α helices projecting from the membrane as the dimer interface in the voltage-gated H^+ channel. *J. Gen. Physiol.* 143:377–386. http://dx.doi.org/10.1085/jgp.201311082

Gonzalez, C., H.P. Koch, B.M. Drum, and H.P. Larsson. 2010. Strong cooperativity between subunits in voltage-gated proton channels. *Nat. Struct. Mol. Biol.* 17:51–56. http://dx.doi.org/10.1038/nsmb.1739

Gonzalez, C., S. Rebolledo, M.E. Perez, and H.P. Larsson. 2013. Molecular mechanism of voltage sensing in voltage-gated proton channels. *J. Gen. Physiol.* 141:275–285. http://dx.doi.org/10.1085/jgp.201210857

Hao, J., F. Padilla, M. Dandonneau, C. Lavebratt, F. Lesage, J. Noël, and P. Delmas. 2013. Kv1.1 channels act as mechanical brake in the senses of touch and pain. *Neuron.* 77:899–914. http://dx.doi.org/10.1016/j.neuron.2012.12.035

Henderson, L.M., J.B. Chappell, and O.T. Jones. 1987. The superoxide-generating NADPH oxidase of human neutrophils is electrogenic and associated with an H^+ channel. *Biochem. J.* 246:325–329. http://dx.doi.org/10.1042/bj2460325

Henry, S.J., C.S. Chen, J.C. Crocker, and D.A. Hammer. 2015. Protrusive and contractile forces of spreading human neutrophils. *Biophys. J.* 109:699–709. http://dx.doi.org/10.1016/j.bpj.2015.05.041

Hondares, E., M.A. Brown, B. Musset, D. Morgan, V.V. Cherny, C. Taubert, M.K. Bhamrah, D. Coe, F. Marelli-Berg, J.G. Gribben, et al. 2014. Enhanced activation of an amino-terminally truncated isoform of the voltage-gated proton channel HVCN1 enriched in malignant B cells. *Proc. Natl. Acad. Sci. USA.* 111:18078–18083. http://dx.doi.org/10.1073/pnas.1411390111

Hong, L., M.M. Pathak, I.H. Kim, D. Ta, and F. Tombola. 2013. Voltage-sensing domain of voltage-gated proton channel Hv1 shares mechanism of block with pore domains. *Neuron.* 77:274–287. http://dx.doi.org/10.1016/j.neuron.2012.11.013

Hong, L., I.H. Kim, and F. Tombola. 2014. Molecular determinants of Hv1 proton channel inhibition by guanidine derivatives. *Proc. Natl. Acad. Sci. USA.* 111:9971–9976. http://dx.doi.org/10.1073/pnas.1324012111

Hong, L., V. Singh, H. Wulff, and F. Tombola. 2015. Interrogation of the intersubunit interface of the open Hv1 proton channel with a probe of allosteric coupling. *Sci. Rep.* 5:14077. http://dx.doi.org/10.1038/srep14077

Houk, A.R., A. Jilkine, C.O. Mejean, R. Boltyanskiy, E.R. Dufresne, S.B. Angenent, S.J. Altschuler, L.F. Wu, and O.D. Weiner. 2012. Membrane tension maintains cell polarity by confining signals to the leading edge during neutrophil migration. *Cell.* 148:175–188. http://dx.doi.org/10.1016/j.cell.2011.10.050

Iovannisci, D., B. Illek, and H. Fischer. 2010. Function of the HVCN1 proton channel in airway epithelia and a naturally occurring mutation, M91T. *J. Gen. Physiol.* 136:35–46. http://dx.doi.org/10.1085/jgp.200910379

Koch, H.P., T. Kurokawa, Y. Okochi, M. Sasaki, Y. Okamura, and H.P. Larsson. 2008. Multimeric nature of voltage-gated proton channels. *Proc. Natl. Acad. Sci. USA.* 105:9111–9116. http://dx.doi.org/10.1073/pnas.0801553105

Kohout, S.C., M.H. Ulbrich, S.C. Bell, and E.Y. Isacoff. 2008. Subunit organization and functional transitions in Ci-VSP. *Nat. Struct. Mol. Biol.* 15:106–108. http://dx.doi.org/10.1038/nsmb1320

Kuno, M., H. Ando, H. Morihata, H. Sakai, H. Mori, M. Sawada, and S. Oiki. 2009. Temperature dependence of proton permeation through a voltage-gated proton channel. *J. Gen. Physiol.* 134:191–205. http://dx.doi.org/10.1085/jgp.200910213

Lacroix, J.J., H.C. Hyde, F.V. Campos, and F. Bezanilla. 2014. Moving gating charges through the gating pore in a Kv channel voltage sensor. *Proc. Natl. Acad. Sci. USA.* 111:E1950–E1959. http://dx.doi.org/10.1073/pnas.1406161111

Laitko, U., P.F. Juranka, and C.E. Morris. 2006. Membrane stretch slows the concerted step prior to opening in a Kv channel. *J. Gen. Physiol.* 127:687–701. http://dx.doi.org/10.1085/jgp.200509394

Lee, S.Y., J.A. Letts, and R. Mackinnon. 2008. Dimeric subunit stoichiometry of the human voltage-dependent proton channel Hv1. *Proc. Natl. Acad. Sci. USA.* 105:7692–7695. http://dx.doi.org/10.1073/pnas.0803277105

Li, Q., S. Wanderling, M. Paduch, D. Medovoy, A. Singharoy, R. McGreevy, C.A. Villalba-Galea, R.E. Hulse, B. Roux, K. Schulten, et al. 2014. Structural mechanism of voltage-dependent gating in

an isolated voltage-sensing domain. *Nat. Struct. Mol. Biol.* 21:244–252. http://dx.doi.org/10.1038/nsmb.2768

Li, Q., R. Shen, J.S. Treger, S.S. Wanderling, W. Milewski, K. Siwowska, F. Bezanilla, and E. Perozo. 2015. Resting state of the human proton channel dimer in a lipid bilayer. *Proc. Natl. Acad. Sci. USA.* 112:E5926–E5935. http://dx.doi.org/10.1073/pnas.1515043112

Li, S.J., Q. Zhao, Q. Zhou, H. Unno, Y. Zhai, and F. Sun. 2010. The role and structure of the carboxyl-terminal domain of the human voltage-gated proton channel Hv1. *J. Biol. Chem.* 285:12047–12054. http://dx.doi.org/10.1074/jbc.M109.040360

Liman, E.R., J. Tytgat, and P. Hess. 1992. Subunit stoichiometry of a mammalian K^+ channel determined by construction of multimeric cDNAs. *Neuron.* 9:861–871. http://dx.doi.org/10.1016/0896-6273(92)90239-A

Lishko, P.V., I.L. Botchkina, A. Fedorenko, and Y. Kirichok. 2010. Acid extrusion from human spermatozoa is mediated by flagellar voltage-gated proton channel. *Cell.* 140:327–337. http://dx.doi.org/10.1016/j.cell.2009.12.053

Long, S.B., E.B. Campbell, and R. Mackinnon. 2005. Crystal structure of a mammalian voltage-dependent *Shaker* family K^+ channel. *Science.* 309:897–903. http://dx.doi.org/10.1126/science.1116269

Maingret, F., M. Fosset, F. Lesage, M. Lazdunski, and E. Honoré. 1999. TRAAK is a mammalian neuronal mechano-gated K^+ channel. *J. Biol. Chem.* 274:1381–1387. http://dx.doi.org/10.1074/jbc.274.3.1381

Marches, R., E.S. Vitetta, and J.W. Uhr. 2001. A role for intracellular pH in membrane IgM-mediated cell death of human B lymphomas. *Proc. Natl. Acad. Sci. USA.* 98:3434–3439. http://dx.doi.org/10.1073/pnas.061028998

Maroto, R., A. Raso, T.G. Wood, A. Kurosky, B. Martinac, and O.P. Hamill. 2005. TRPC1 forms the stretch-activated cation channel in vertebrate cells. *Nat. Cell Biol.* 7:179–185. http://dx.doi.org/10.1038/ncb1218

Masters, T.A., B. Pontes, V. Viasnoff, Y. Li, and N.C. Gauthier. 2013. Plasma membrane tension orchestrates membrane trafficking, cytoskeletal remodeling, and biochemical signaling during phagocytosis. *Proc. Natl. Acad. Sci. USA.* 110:11875–11880. http://dx.doi.org/10.1073/pnas.1301766110

McGrail, D.J., Q.M. Kieu, J.A. Iandoli, and M.R. Dawson. 2015. Actomyosin tension as a determinant of metastatic cancer mechanical tropism. *Phys. Biol.* 12:026001. http://dx.doi.org/10.1088/1478-3975/12/2/026001

Mongin, A.A. 2007. Disruption of ionic and cell volume homeostasis in cerebral ischemia: The perfect storm. *Pathophysiology.* 14:183–193. http://dx.doi.org/10.1016/j.pathophys.2007.09.009

Mony, L., T.K. Berger, and E.Y. Isacoff. 2015. A specialized molecular motion opens the Hv1 voltage-gated proton channel. *Nat. Struct. Mol. Biol.* 22:283–290. http://dx.doi.org/10.1038/nsmb.2978

Morgan, D., V.V. Cherny, R. Murphy, B.Z. Katz, and T.E. DeCoursey. 2005. The pH dependence of NADPH oxidase in human eosinophils. *J. Physiol.* 569:419–431. http://dx.doi.org/10.1113/jphysiol.2005.094748

Morgan, D., V.V. Cherny, A. Finnegan, J. Bollinger, M.H. Gelb, and T.E. DeCoursey. 2007. Sustained activation of proton channels and NADPH oxidase in human eosinophils and murine granulocytes requires PKC but not $cPLA_2\alpha$ activity. *J. Physiol.* 579:327–344. http://dx.doi.org/10.1113/jphysiol.2006.124248

Mori, H., H. Sakai, H. Morihata, J. Kawawaki, H. Amano, T. Yamano, and M. Kuno. 2003. Regulatory mechanisms and physiological relevance of a voltage-gated H^+ channel in murine osteoclasts: phorbol myristate acetate induces cell acidosis and the channel activation. *J. Bone Miner. Res.* 18:2069–2076. http://dx.doi.org/10.1359/jbmr.2003.18.11.2069

Morihata, H., F. Nakamura, T. Tsutada, and M. Kuno. 2000. Potentiation of a voltage-gated proton current in acidosis-induced swelling of rat microglia. *J. Neurosci.* 20:7220–7227.

Morris, C.E., E.A. Prikryl, and B. Joós. 2015. Mechanosensitive gating of Kv channels. *PLoS One.* 10:e0118335. http://dx.doi.org/10.1371/journal.pone.0118335

Murata, Y., H. Iwasaki, M. Sasaki, K. Inaba, and Y. Okamura. 2005. Phosphoinositide phosphatase activity coupled to an intrinsic voltage sensor. *Nature.* 435:1239–1243. http://dx.doi.org/10.1038/nature03650

Musset, B., D. Morgan, V.V. Cherny, D.W. MacGlashan Jr., L.L. Thomas, E. Ríos, and T.E. DeCoursey. 2008. A pH-stabilizing role of voltage-gated proton channels in IgE-mediated activation of human basophils. *Proc. Natl. Acad. Sci. USA.* 105:11020–11025. http://dx.doi.org/10.1073/pnas.0800886105

Musset, B., M. Capasso, V.V. Cherny, D. Morgan, M. Bhamrah, M.J. Dyer, and T.E. DeCoursey. 2010a. Identification of Thr29 as a critical phosphorylation site that activates the human proton channel Hvcn1 in leukocytes. *J. Biol. Chem.* 285:5117–5121. http://dx.doi.org/10.1074/jbc.C109.082727

Musset, B., S.M. Smith, S. Rajan, V.V. Cherny, S. Sujai, D. Morgan, and T.E. DeCoursey. 2010b. Zinc inhibition of monomeric and dimeric proton channels suggests cooperative gating. *J. Physiol.* 588:1435–1449. http://dx.doi.org/10.1113/jphysiol.2010.188318

Nordström, T., O.D. Rotstein, R. Romanek, S. Asotra, J.N. Heersche, M.F. Manolson, G.F. Brisseau, and S. Grinstein. 1995. Regulation of cytoplasmic pH in osteoclasts. Contribution of proton pumps and a proton-selective conductance. *J. Biol. Chem.* 270:2203–2212. http://dx.doi.org/10.1074/jbc.270.5.2203

O'Hanlon, D.E., T.R. Moench, and R.A. Cone. 2013. Vaginal pH and microbicidal lactic acid when lactobacilli dominate the microbiota. *PLoS One.* 8:e80074. http://dx.doi.org/10.1371/journal.pone.0080074

Patel, A.J., E. Honoré, F. Maingret, F. Lesage, M. Fink, F. Duprat, and M. Lazdunski. 1998. A mammalian two pore domain mechano-gated S-like K^+ channel. *EMBO J.* 17:4283–4290. http://dx.doi.org/10.1093/emboj/17.15.4283

Pathak, M.M., J.L. Nourse, T. Tran, J. Hwe, J. Arulmoli, D.T. Le, E. Bernardis, L.A. Flanagan, and F. Tombola. 2014. Stretch-activated ion channel Piezo1 directs lineage choice in human neural stem cells. *Proc. Natl. Acad. Sci. USA.* 111:16148–16153. http://dx.doi.org/10.1073/pnas.1409802111

Payandeh, J., T. Scheuer, N. Zheng, and W.A. Catterall. 2011. The crystal structure of a voltage-gated sodium channel. *Nature.* 475:353–358. http://dx.doi.org/10.1038/nature10238

Pupo, A., and C. Gonzalez León. 2014. In pursuit of an inhibitory drug for the proton channel. *Proc. Natl. Acad. Sci. USA.* 111:9673–9674. http://dx.doi.org/10.1073/pnas.1408808111

Qiu, F., S. Rebolledo, C. Gonzalez, and H.P. Larsson. 2013. Subunit interactions during cooperative opening of voltage-gated proton channels. *Neuron.* 77:288–298. http://dx.doi.org/10.1016/j.neuron.2012.12.021

Ramsey, I.S., M.M. Moran, J.A. Chong, and D.E. Clapham. 2006. A voltage-gated proton-selective channel lacking the pore domain. *Nature.* 440:1213–1216. http://dx.doi.org/10.1038/nature04700

Ramsey, I.S., Y. Mokrab, I. Carvacho, Z.A. Sands, M.S. Sansom, and D.E. Clapham. 2010. An aqueous H^+ permeation pathway in the voltage-gated proton channel Hv1. *Nat. Struct. Mol. Biol.* 17:869–875. http://dx.doi.org/10.1038/nsmb.1826

Sasaki, M., M. Takagi, and Y. Okamura. 2006. A voltage sensor-domain protein is a voltage-gated proton channel. *Science.* 312:589–592. http://dx.doi.org/10.1126/science.1122352

Schmidt, D., J. del Mármol, and R. MacKinnon. 2012. Mechanistic basis for low threshold mechanosensitivity in voltage-dependent K^+ channels. *Proc. Natl. Acad. Sci. USA*. 109:10352–10357. http://dx.doi.org/10.1073/pnas.1204700109

Seredenina, T., N. Demaurex, and K.H. Krause. 2015. Voltage-gated proton channels as novel drug targets: From NADPH oxidase regulation to sperm biology. *Antioxid. Redox Signal.* 23:490–513. http://dx.doi.org/10.1089/ars.2013.5806

Siesjö, B.K., K. Katsura, and T. Kristián. 1996. Acidosis-related damage. *Adv. Neurol.* 71:209–233.

Song, M., and S.P. Yu. 2014. Ionic regulation of cell volume changes and cell death after ischemic stroke. *Transl. Stroke Res.* 5:17–27. http://dx.doi.org/10.1007/s12975-013-0314-x

Tabarean, I.V., and C.E. Morris. 2002. Membrane stretch accelerates activation and slow inactivation in Shaker channels with S3-S4 linker deletions. *Biophys. J.* 82:2982–2994. http://dx.doi.org/10.1016/S0006-3495(02)75639-7

Takeshita, K., S. Sakata, E. Yamashita, Y. Fujiwara, A. Kawanabe, T. Kurokawa, Y. Okochi, M. Matsuda, H. Narita, Y. Okamura, and A. Nakagawa. 2014. X-ray crystal structure of voltage-gated proton channel. *Nat. Struct. Mol. Biol.* 21:352–357. http://dx.doi.org/10.1038/nsmb.2783

Tao, X., A. Lee, W. Limapichat, D.A. Dougherty, and R. MacKinnon. 2010. A gating charge transfer center in voltage sensors. *Science.* 328:67–73. http://dx.doi.org/10.1126/science.1185954

Tombola, F., M.H. Ulbrich, and E.Y. Isacoff. 2008. The voltage-gated proton channel Hv1 has two pores, each controlled by one voltage sensor. *Neuron.* 58:546–556. http://dx.doi.org/10.1016/j.neuron.2008.03.026

Tombola, F., M.H. Ulbrich, S.C. Kohout, and E.Y. Isacoff. 2010. The opening of the two pores of the Hv1 voltage-gated proton channel is tuned by cooperativity. *Nat. Struct. Mol. Biol.* 17:44–50. http://dx.doi.org/10.1038/nsmb.1738

Villalba-Galea, C.A. 2014. Hv1 proton channel opening is preceded by a voltage-independent transition. *Biophys. J.* 107:1564–1572. (published erratum appears in *Biophys. J.* 2014. 107:2477) http://dx.doi.org/10.1016/j.bpj.2014.08.017

Wang, Y., S.J. Li, J. Pan, Y. Che, J. Yin, and Q. Zhao. 2011. Specific expression of the human voltage-gated proton channel Hv1 in highly metastatic breast cancer cells, promotes tumor progression and metastasis. *Biochem. Biophys. Res. Commun.* 412:353–359. http://dx.doi.org/10.1016/j.bbrc.2011.07.102

Wang, Y., S.J. Li, X. Wu, Y. Che, and Q. Li. 2012. Clinicopathological and biological significance of human voltage-gated proton channel Hv1 protein overexpression in breast cancer. *J. Biol. Chem.* 287:13877–13888. http://dx.doi.org/10.1074/jbc.M112.345280

Wood, M.L., E.V. Schow, J.A. Freites, S.H. White, F. Tombola, and D.J. Tobias. 2012. Water wires in atomistic models of the Hv1 proton channel. *Biochim. Biophys. Acta.* 1818:286–293. http://dx.doi.org/10.1016/j.bbamem.2011.07.045

Wu, L.J., G. Wu, M.R. Akhavan Sharif, A. Baker, Y. Jia, F.H. Fahey, H.R. Luo, E.P. Feener, and D.E. Clapham. 2012. The voltage-gated proton channel Hv1 enhances brain damage from ischemic stroke. *Nat. Neurosci.* 15:565–573. http://dx.doi.org/10.1038/nn.3059

Xiong, Z.G., X.M. Zhu, X.P. Chu, M. Minami, J. Hey, W.L. Wei, J.F. MacDonald, J.A. Wemmie, M.P. Price, M.J. Welsh, and R.P. Simon. 2004. Neuroprotection in ischemia: blocking calcium-permeable acid-sensing ion channels. *Cell.* 118:687–698. http://dx.doi.org/10.1016/j.cell.2004.08.026

Zhang, X., W. Ren, P. DeCaen, C. Yan, X. Tao, L. Tang, J. Wang, K. Hasegawa, T. Kumasaka, J. He, et al. 2012. Crystal structure of an orthologue of the NaChBac voltage-gated sodium channel. *Nature.* 486:130–134.